Journal of Non-Newtonian Fluid Mechanics 175-176 (2012) 64–75

Contents lists available at SciVerse ScienceDirect

Journal of Non-Newtonian Fluid Mechanics

journal homepage: http://www.elsevier.com/locate/jnnfm

Effect of viscoelasticity on liquid transfer during gravure printing

Ashwin K. Sankaran, Jonathan P. Rothstein *

Department of Mechanical and Industrial Engineering, University of Massachusetts – Amherst, 160 Governors Drive, Amherst, Massachusetts 01003, United States

ARTICLE INFO

Article history:
Received 14 February 2012
Received in revised form 22 March 2012
Accepted 23 March 2012
Available online 30 March 2012

Keywords:
Viscoelasticity
Gravure printing
Pickout process
Extensional rheology
Coating

ABSTRACT

Roll-to-roll patterning of small-scale features on a rapidly moving web is an industrially important process with a wide array of commercial applications both old and new. Examples include magazine printing and more recently the pattering of flexible electronics. Among the many existing web coating techniques for large-scale fabrication, slit die and gravure coating are the most commonly used. In gravure coating, an engraved roller with a regular array of shallow cavities/cells is used to pick up fluid from a bath. It is then passed through a flexible doctoring blade in order to meter off excess fluid before printing the fluid onto a flexible substrate. Here we present an experimental investigation into the effect that viscoelasticity has on the dynamics of liquid transfer from an idealized gravure cell to a flat rigid substrate. Although the dynamics of the actual gravure coating process is quite complex, we chose to study a simplified process by imposing an extensional flow using a modified filament stretching rheometer in which one of the endplates is replaced by a cell containing a single truncated conical gravure cell. The deformation and stretching of the resulting liquid bridges, the motion of the contact line within the gravure cell and the total amount of fluid removed from the gravure cell are studied as a function of the imposed stretch rate, the fluid rheology, and the geometry of the gravure cell. Two different viscoelastic solutions of high molecular weight polyethylene oxide in water were studied and compared to a series of Newtonian fluids. The results show that the primary impact of viscoelasticity is the addition of an elastic stress which increases the tension along the liquid bridge and significantly increases the bridge lifetime. For stretches where the gravure cell was placed on the bottom and the top plate moved vertically, viscoelasticity was found to significantly reduce the amount of fluid transferred to the top plate. However, by placing the gravure cell on top and reversing the relative direction of the inertial and gravitational stresses, viscoelasticity was found to significantly increase the amount of fluid transferred. Increasing the stretch rate was found to amplify these observations. Finally, increasing the contact angle between the fluid and the gravure cell and decreasing the aspect ratio of the gravure cell were both found to increase the amount of fluid transferred.

1. Introduction

The rapid printing and patterning of small features and the deposition of uniform thin films through roll-to-roll processing is of great importance to a variety of both old and new industries [1,2]. Classically, these printing techniques have been used to produce newspapers and magazines, but more recently they have been extended to manufacture solar panel, electronics, opto-electronics and functional materials. Among the many existing web coating and printing techniques for large-scale fabrication such as slit, roll, dip and gravure are the most commonly used. Each of these techniques has a unique set of advantages and disadvantages. The gravure process has been used widely for printing magazines, tapes and packaging [3]. The primary advantage of roll-to-roll processing that is large areas of coated/printed films can be processed quickly at low manufacturing costs. This has been known for quite some time in traditional printing industries, but has now become of particular interest to the electronics industry who have begun to use an offset gravure printing mechanism to print electronic components [4]. In addition, a host of researchers have been investigating the adaptation of a number of water-based processing techniques like nano-inprint lithography and optical lithography techniques to web-based platforms [1].

A gravure roll-to-roll coater employs two rollers and a doctoring blade. An engraved roller is used to pick up fluid from a bath which passes through a flexible doctoring blade which meters off excess fluid. The engraved roller deposits the fluid from the cells onto the flexible substrate which is held in tension by another roller. An offset gravure process has an intermediate roller between the engraved roller and the substrate. Typical gravure cell sizes have a width ranging from 50 μm to several hundred microns and depths in similar ranges [5,6]. A number of these cells are placed in an array on the engraved roller to print patterned arrays or coat films.

* Corresponding author.
E-mail address: rothstein@ecs.umass.edu (J.P. Rothstein).

0377-0257/$ - see front matter © 2012 Elsevier B.V. All rights reserved.
http://dx.doi.org/10.1016/j.jnnfm.2012.03.011

During the gravure printing process a liquid bridge is formed between the cell and the substrate that is being coated or printed on. This bridge plays an important role in the liquid transfer process from the cell on to the substrate. The physics of the pickout process from a cell is extremely complex resulting in the stretching of a liquid bridge with strong shear and elongational flow components [7]. It is also strongly influenced by the surface properties of the cell and substrate, the limiting parameters being the contact angle between the liquid bridge and both the substrates and moving contact lines that are often pinned by the geometry of the cell [8]. There has been a many studies looking into the dynamics of liquid bridge stretching in detail [9]. The main forces that act on the bridge arise from viscosity and surface tension. The former is stabilizing and latter destabilizing. Due to high curvature of the bridge near the gravure cell and the substrate, the bridge tends to break up at the ends rather than the middle. This results in the formation of two sessile drops on either surfaces and one dynamic drop as the liquid bridge pinches off. The dynamic drop will land on either the substrate or the gravure cell depending upon the orientation of the printing system. If it were to land on the substrate it would cause a hazy print know as misting thereby reducing the quality of the print. In most cases, not all the ink is transferred from the engraved roller on to the substrate. This can in turn become a major problem because residual inks can evaporate leaving behind particulates and dissolved polymers which accumulate within the cell over time and require frequent cleaning. Clogged cells can also cause non-uniform film thickness and reduce print quality.

A number of recent article have investigated both experimentally and computationally the gravure printing process [4,5,8–22]. In some of the earliest computational work, Powell et al. [9] simulating the printing process for a Newtonian liquid from a trapezoidal cavity. The configuration of their simulation is similar to the initial experiments reported in this paper. The gravure cell is placed upside down and a downward velocity is imposed on the substrate to simulate the printing process. In this particular configuration of the cell, gravity assists the emptying process. The authors assumed that the contact lines move down along the sidewalls of the gravure cell and pinned at the bottom internal corner of the cell. They found that by increasing the substrate speed, a longer-lived filament between the cavity and the substrate was formed which in turn facilitated more removal of the fluid from the cavity. Schwartz et al. [19] presented a 2D numerical model for liquid withdrawal from cavities in gravure coating. They restricted the model to the fluid beneath the moving contact line and studied the effect of gravitational drainage for both a Newtonian and a shear thinning fluid. Small gravure cells were found to retain a large volume of liquid for extended periods of time. Schwartz [20] further investigated the effect of gravure cell shape and patterns of gravure cells on the pickout. Yin and Kumar later [21,22] studied the gravure printing process by simulating a single isolated gravure cell. They assumed the lubrication approximation for a flow between the cavity and a flexible wall and used a 1D model to investigate the effect of web flexibility on the pressure profiles inside the gravure cell. They conclude that some amount of flexibility is needed to effectively remove fluid from the cell.

Previous experimental studies have separated the process into touchdown, shear and pickout [18,22]. In this paper and many others, the emphasis has been on the pickout process. In their recent experiments, Yin and Kumar [22] used a glass top plate moving over a scaled up gravure cell to look into the flow dynamics that occur during the emptying of the cell. They measured the amount of fluid removed from the gravure cell as a function of capillary number by using different water/glycerol fluids. The amount of fluid removed, or pickout, was found to decrease with increasing capillary number for a trapezoidal cavity of aspect ratio greater than one. Later, Hoda and Kumar [14] simulated the removal of a Newtonian liquid from a model gravure cell, they also observe that volume of liquid left in the cell behind decreases as the capillary number decreases. They were also the first to point out the importance of moving contact lines, contact angles and the normal velocity component to the cell on the amount of liquid removed. They demonstrated that imposing a normal velocity enhances the rate of emptying and removal of liquid from the cavity. Above a critical normal velocity the cells were found to completely empty. This result highlights the importance of strong elongational flow during the emptying process. A later work from Kumar's group [11] numerically investigated the slipping of contact lines in stretching of liquid bridges from an axisymmetric cavity. The fluid removal was found to increase as contact angle of the gravure cell increases and the contact angle made with the substrate decreases. They also pointed out the significance of the position of the contact line inside the gravure cell. Wider cavities were found to be capable of transferring more liquid from the gravure cells. This is because they facilitated contact line slipping down the wall of the cell before the contact line eventually pinned at the bottom of the cell. The effect of inertia and contact angle on the amount of liquid transfer from trapezoidal cavity and flat plates was investigated by Dodds et al. [12]. Variation of contact angle and inertia were found to affect for the formation of a satellite drop in the presence of cavity or a flat plate. As discussed later in this paper, the breakup of the liquid bridge is accelerated in the presence of the cavity due to higher curvature; hence the symmetry of breakup is very much dependent on the contact angles and inertia. A number of other studies have also investigated the role of cell geometry and wettability on printing and coating. Huang et al. [15] studied the amount of liquid transferred from a trapezoidal cavity onto a moving plate by varying the contact angles, initial distance and cavity shape. They used a freely moving contact line and demonstrated that the evolution of the contact line in the cell is strongly dependent on the contact angle between the liquid and the cell. Kang et al. [16] studied the effect of contact angle on the liquid transfer between two separating flat plates. They found that by increasing the contact angle of the bottom and reducing the contact angle on the top plate more liquid can be transferred onto the moving substrate.

Inks, color pigments and other organic compounds commonly exhibit a non-Newtonian flow behavior due to the presence of colloidal particles and high molecular weight additives. Even though non-Newtonian fluids should respond differently in the complex flows involved in gravure printing, very little in known about how the rheology of the printing liquid affects pickout as all the studies available are all numerical simulations [10,13,15]. Huang et al. [15] showed that a shear thinning accelerates the breakup of the liquid bridge and concluded that viscoelasticity in inks plays a major role in the transfer process. Ahn et al. [10] modeled an elastic fluid using an Oldroyd-B model at a Weissenberg number of $Wi = \lambda\dot{\gamma} = 0.15$. The Weissenberg number is defined as the product of the fluid relaxation time, λ, and shear rate imposed, $\dot{\gamma}$. They computed velocity and pressure fields inside the gravure cell, even at low Weissenberg numbers the effect of elasticity was found to be significant as the pressure gradient between the gravure roll and the web increases by a factor of three. This work highlights the need to consider elasticity in the ink transfer from gravure cells. Ghadiri et al. [13] used a Carreau model to represent a non-Newtonian ink and optimized the geometry of the gravure cell. The optimized geometry yielded over 90% liquid removal from the cavity. Side wall angle and the depth of the cavity was found to play a crucial role in the emptying process, a shallow cavity removed more fluid, whereas the side wall angle showed symmetry about 45° [10].

Due to the primarily extensional nature of these flows, the elongational rheology of the coating fluids is a critical parameter to be

considered. In this paper, we aim to qualitatively and quantitatively understand the effect of fluid elasticity on the effectiveness and efficiency of an idealized gravure printing process. We used a scaled up idealized gravure cell to make direct measurements of the liquid transferred from the gravure cell. Using high-speed video, we visualized the dynamics of the stretching of the liquid bridge from the gravure cell. Using variations of our experimental setup we independently studied the effect of gravity, inertia, cell geometry, viscoelasticity and wettability.

2. Experimental setup

In our experiments we used a modified version of a capillary breakup rheometer to emulate the pickout process for a scaled up idealized gravure cell. The initial conditions of the experiment are static. We do not emulate the touchdown and the shearing process that would occur in the real roll-to-roll coating. This is a fundamental study to understand the essential parameters involved in the pickout of viscoelastic gravure printing for an idealized geometry.

The apparatus used shown in Fig. 1 was used in our experiments. It consists of a computer-controlled linear motor that was attached to a stainless steel plate which is in-line with the gravure cell. We vertically stretched the fluid using a linear motor LinMot PO1. Because we impose only a normal velocity component to the fluid inside the gravure cell, there is no shearing of the fluid in the tangential direction. Three configurations were investigated to independently study the effects of inertia, gravity and capillary thinning. As seen in Fig. 2, these configurations include the gravure cell locked on the top and bottom substrate. The gravure cell is fabricated by casting a mixture of PDMS/crosslinker onto a mold machined in stainless steel. Two different molds were fabricated both had a sidewall angle of $\alpha = 15^\circ$ and a cell radius of $R = 2.5$mm, moreover, the two molds were machined to produce cells of different depths, $h = 1$mm and $h = 0.5$mm respectively. The cell was positioned using a three dimensional stage which was used to precisely adjust the position of the cell to align with the opposite plate.

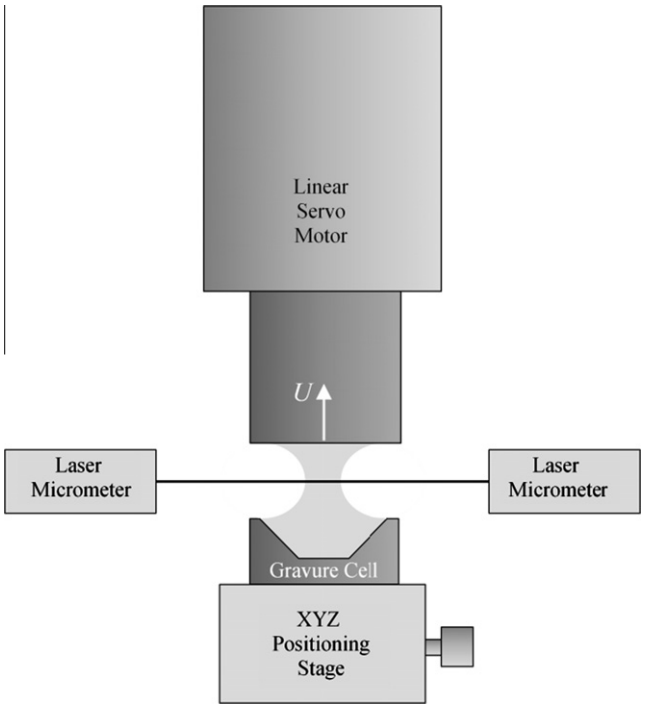

Fig. 1. Schematic diagram of experimental setup used for idealized gravure cell study.

Initially a cylindrical fluid filament was held between the plate and cell, the separation, L_i , was kept constant at an aspect ratio of $L_i/R = 0.3$. The plate was then moved at a constant velocity normal to cell subjecting the fluid filament to a strong elongational flow. A liquid bridge was formed between the moving plate and the gravure cell which progressively decreased in radius and eventually broke. For a Newtonian fluid, one sessile drop and two static drops on the plate and inside the cell were formed. For a viscoelastic fluid there was a long-lived filament between the plate and cell which eventually thins under capillary drainage and breaks. The final stretch distance was held constant for all the experiments at an aspect ratio of $L_f/R = 12$ and the speed was varied from $2\ \text{mm/s} < U < 190\ \text{mm/s}$. The mass of the fluid remaining in the gravure cell was measured using a high precision weight balance and the pickout was then defined as the ratio of the mass of fluid removed from the cell to the initial mass of fluid inside the cell. After each stretch, the cell was cleaned and dried before starting the next stretch. The experimentally measure values of pickout were with an uncertainty of just 2%.

2.1. Test fluids

The test fluids were polyethylene oxide (PEO) solutions of various molecular weights dissolved in water. The PEO was obtained from Aldrich Chemicals. The PEO was mixed with water and stirred for 24 h to obtain a homogenous solution. Three Newtonian test fluids and two viscoelastic test fluids were used in the experiments described here. The Newtonian fluids were 10 wt%, 15 wt% and 20 wt% solution of 2×10^4 g/mol PEO in water. These lower molecular weight PEO samples will be designated 20K PEO. The lower molecular weight PEO was used to increase the viscosity of the solution without adding significant elasticity. The two viscoelastic fluids, designated 2M PEO and 8M PEO, each contained the same 20 wt% of 2×10^4 g/mol PEO, but with an additional 0.16 wt% of either 2×10^6 g/mol PEO or 8×10^6 g/mol PEO respectively to increase the elasticity of the final solution.

The surface tension was measured by a standard pendant drop method. The drop profile was fitted to Young–Laplace equation. Transient and steady state values of surface tension were measured and found to be consistent over a number of trials. The results of the surface tension measurements of each fluid are presented in Table 1. In addition, advancing and receding contact angle measurements between the fluids and the PDMS used to fabricate the idealized gravure cells used in the following experiments were measured to be $\theta_a = 90^\circ$ and $\theta_r = 50^\circ$. The advancing contact angles between the fluid and the aluminum top plate was found to be $\theta_a = 15^\circ$, however, the receding contact angle was difficult to measure and could only be determined to be less than $\theta_r < 10^\circ$.

2.2. Shear rheology

A stress controlled rotational rheometer TA Advantage 2000 with a cone-and-plate geometry was used to characterize the fluid in steady state and oscillatory shear flow. The steady shear rheology of each solution is presented in Fig. 3. For all three solutions, the shear viscosity was found to remain essentially constant over the shear rate range studied. The addition of the high molecular weight PEO was found to increase the shear viscosity, but not result in any shear thinning. The linear viscoelasticity of these samples was also measured through small amplitude oscillatory shear measurements, however, due to the relatively low viscosity and the very small relaxation time of the fluids little useful information could be gathered from these measurements.

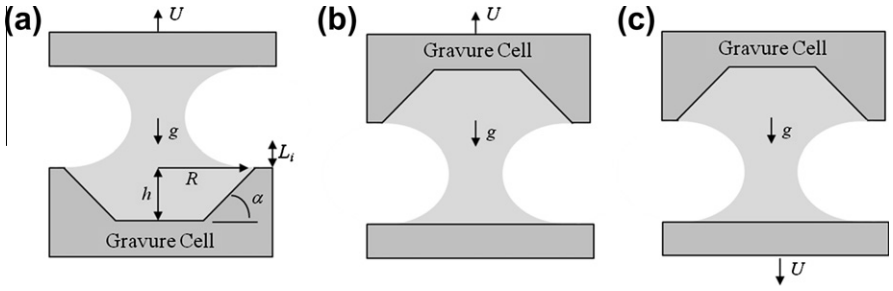

Fig. 2. Schematic diagram showing the three different gravure cell configurations. Note that in all cases the initial aspect ratio is fixed at $L_i/R = 0.3$.

Table 1
Rheological and physical properties of test fluids used in gravure experiments. Note that c^* is the overlap concentration of the polymers.

Solution	Mw of PEO (kg/mol)	c/c^*	λ_E (s)	Surface tension (mN/m)	Zero shear viscosity (Pa s)	Steady extensional viscosity (Pa s)
20 wt% 20K PEO	20	0.011		52	0.0567	
15 wt% 20K PEO	20	0.008		58	0.0263	
10 wt% 20K PEO	20	0.005		62	0.0106	
2M PEO	2000	0.186	0.021	58	0.170	575
8M PEO	8000	0.459	0.210	58	0.227	175

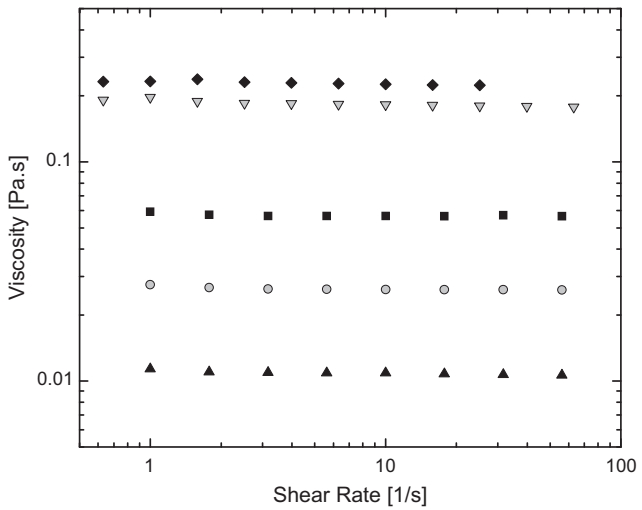

Fig. 3. Steady shear viscosity measurements of the test fluids as a function of shear rate. The data include: (■) 20% 20K PEO, (•)15% 20K PEO, (▲) 10% 20K PEO, (▼) 2M PEO and (◆) 8M PEO.

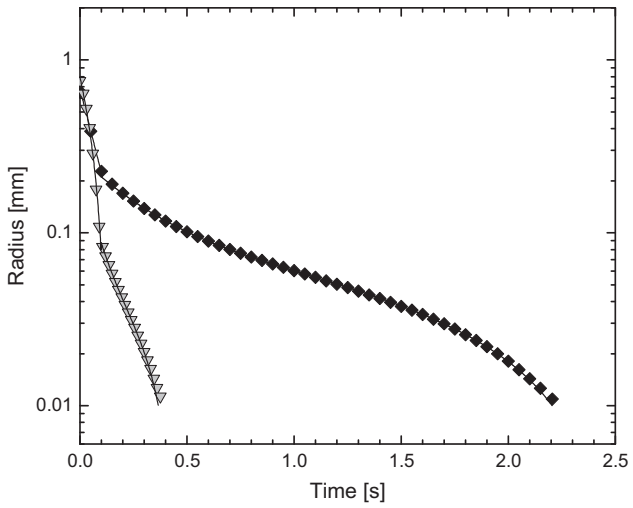

Fig. 4. Radius evolution as a function of time during a capillary breakup extensional rheology measurement. The data include: (▼) 2M PEO and (◆) 8M PEO. Additionally, a fit using Eq. (3) is superimposed over each dataset.

2.3. Capillary breakup extensional rheology measurements

Capillary breakup extensional rheometry (CaBER) measurements have become an increasingly common technique for determining the extensional rheology of the less concentrated and less viscous fluids [23–32]. The capillary breakup extensional rheometry measurements presented here were performed using the high-speed CaBER designed and developed for these experiments shown in Fig. 1. In all of the capillary breakup extensional rheometer (CaBER) experiments presented here, an initial nearly cylindrical fluid sample is placed between two cylindrical plates and stretched with a constant velocity of $U = 200$ mm/s from an initial length $L_i = R$ to final length of L_f. In these experiments the final stretch length is fixed at $L_f = 5\ L_i$. The stretch is then stopped and the capillary thinning of the liquid bridge formed between the two endplates produces a uniaxial extensional flow that can be used to measure an apparent extensional viscosity of the test fluid.

The breakup of the fluid filament is driven by capillary stresses and resisted by the viscous and extensional stresses developed within the flow. The extensional viscosity of a complex liquid solution can be determined by measuring the change in the filament diameter as a function of time. Papageorgiou [33] showed that for a Newtonian fluid of extensional viscosity η_E the radius of the fluid filament will decay linearly with time, $R_{mid}(t) \propto (t_b - t)/\eta_E$, to the final breakup at t_b. Conversely, Entov and Hinch [27] showed that for an Oldroyd-B fluid with an extensional relaxation time, λ_E, the radius will decay exponentially with time, $R_{mid}(t) \propto \exp(-t/3\lambda_E)$, resulting in a constant extension rate of the fluid filament given by

$$\dot{\varepsilon} = -\frac{2}{R_{mid}(t)}\frac{dR_{mid}(t)}{dt} = \frac{2}{3\lambda_E}, \tag{1}$$

and hence for an Oldroyd-B fluid, the flow has a constant Weissenberg number of $Wi = \lambda_E\dot{\varepsilon} = 2/3$. This value is larger than the critical Weissenberg number of $Wi = 1/2$ needed to achieve coil-stretch transition and thus the uniaxial extension should be fast enough to produce strain hardening of the extensional viscosity for the high molecular weight polymer solutions. The evolution of an *apparent* extensional viscosity with this extension rate profile can easily be

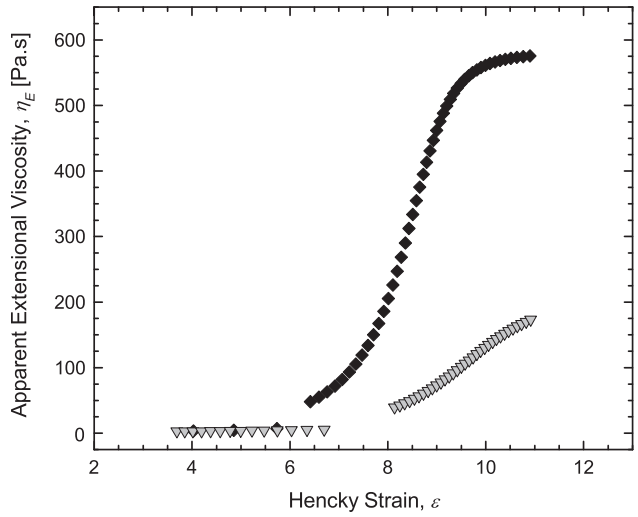

Fig. 5. Apparent extensional viscosity as a function of Hencky strain. The data include: (▼) 2M PEO and (◆) 8M PEO.

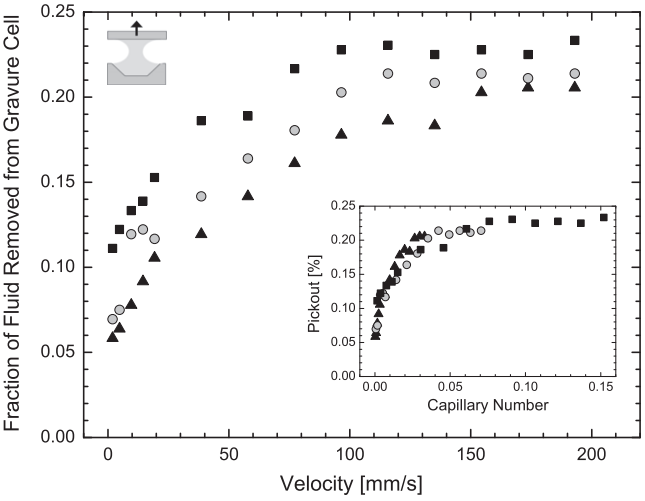

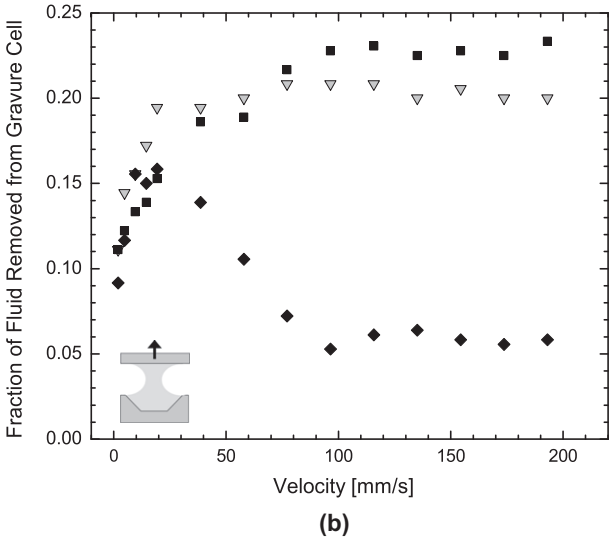

Fig. 6. Fraction of fluid removed from the gravure cell (pickout) as a function of velocity for the configuration where the gravure cell is stationary and placed on the bottom plate. The data include: (■) 20% 20K PEO, (•)15% 20K PEO, (▲) 10% 20K PEO, (▼) 2M PEO and (◆) 8M PEO.

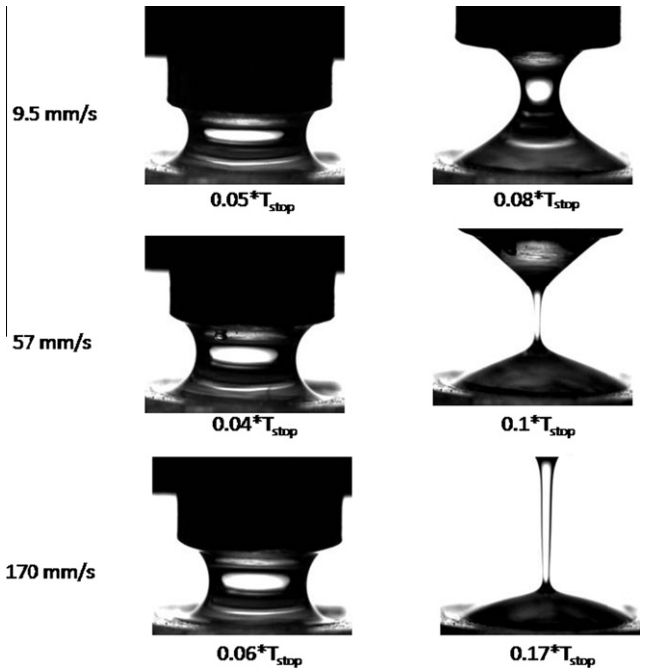

Fig. 7. Time series of images of 20% 20K PEO dewetting when the gravure cell is held stationary as the bottom plate. Time is non-dimensionalized with the time that the top plate reaches the end of its travel and stops, T_{stop}. For the three stretch velocities shown here from top to bottom, T_{stop} = 3.2 s, 0.53 s and 0.18 s.

calculated by applying a force balance between capillary stresses and the viscous and elastic tensile stresses within the fluid filament [24]

$$\eta_E = \frac{\sigma/R_{mid}(t)}{\dot{\varepsilon}(t)} = \frac{-\sigma}{dD_{mid}/dt}. \tag{2}$$

To calculate the apparent extensional viscosity, the diameter measurements can either be fit with a spline and then differentiated or, for more well-defined fluids, the diameter can first be fit with an appropriate functional form and then be differentiated with respect to time. For the case of viscoelastic systems where the elastic component reaches a finite extensibility, Anna and McKinley [24] proposed the following fitting function:

$$D_{mid}(t) = Ae^{-Bt} - Ct + E. \tag{3}$$

For both the 2M PEO and 8M PEO solutions, the diameter decay presented in Fig. 4 is well fit by a Newtonian response at small times and the FENE-P model response at large times. The diameter profile was then differentiated with time and inserted into Eq. (2), the resulting extensional viscosity of each solution is shown in Fig. 5. The discontinuity in the extensional viscosity data is due to fitting the diameter decay data in Fig. 4 with different models at early and long times. At early times, both fluids show expected Newtonian response and an extensional viscosity of $\eta_E \simeq 3\eta_0$. At long times, as the extensional rate increases, each solution clearly shows a strong extensional thickening resulting in Trouton ratios, $Tr = \eta_E/\eta_0 > 1000$ in each case. As expected, the higher molecular weight sample, 8M PEO, demonstrates significantly more extensional thickening than the lower molecular weight sample, 2M PEO. Additionally, it is important to note that the extensional viscosity of the 20K PEO was too small to measure with our CaBER device. The choices of fitting parameters in Eq. (3) have some physical relevance. The exponential decay of the fluid filament diameter at intermediate times can be related to the extensional relaxation time and the fitting parameter B such that $B = 1/3\lambda_E$. For dilute polymer solution systems, this extensional relaxation time can be

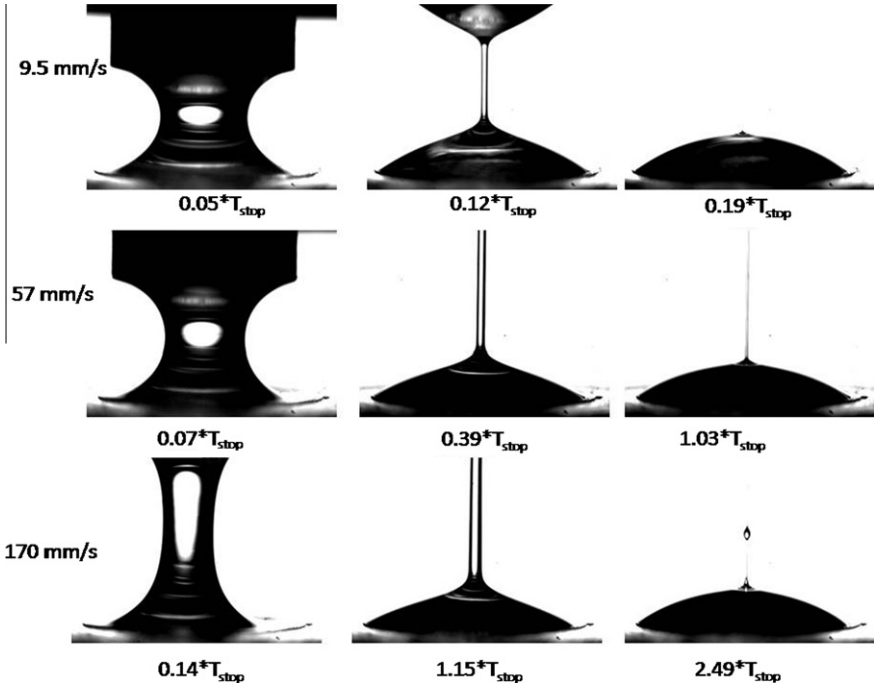

Fig. 8. Time series of images of 2M PEO dewetting when the gravure cell is held stationary as the bottom plate. Time is non-dimensionalized with the time that the top plate reaches the end of its travel and stops, T_{stop}. For the three stretch velocities shown here from top to bottom, T_{stop} = 3.2 s, 0.53 s and 0.18 s.

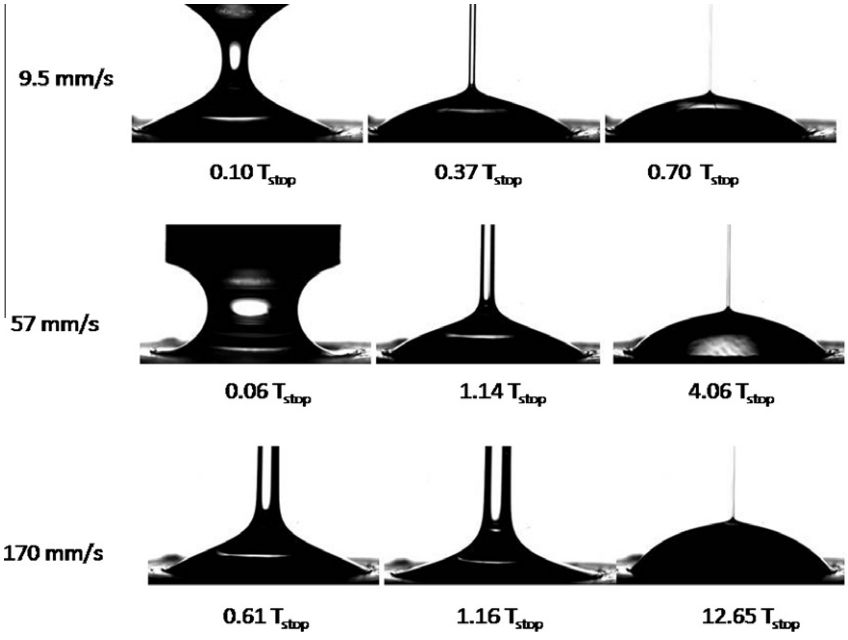

Fig. 9. Time series of images of 8M PEO dewetting when the gravure cell is held stationary as the bottom plate. Time is non-dimensionalized with the time that the top plate reaches the end of its travel and stops, T_{stop}. For the three stretch velocities shown here from top to bottom, T_{stop} = 3.2 s, 0.53 s and 0.18 s.

much larger than the shear relaxation time [30]. For both the 8M PEO and 2M PEO solutions tested here, the relaxation time was too small to be measured from the small amplitude oscillatory shear measurements and could only be characterized in extension. The extensional relaxation time is listed in Table 1. Additionally, C can be related to the equilibrium value of the extensional viscosity at late times, $\eta_{E,\infty}$, when the finite extensibility limit of the polymer is reached, such that $C = 0.7127\sigma/\eta_{E,\infty}$ [33]. A list of the extensional relaxation time and the steady state extensional viscosities are also presented in Table 1.

3. Results and discussion

3.1. Printing with gravure cell on the bottom and stationary

In the first set of experiments, the deeper (h = 1 mm) gravure cell was placed on the bottom and stretched the fluid against the direction of gravity by pulling the top plate upwards at a constant velocity (Fig. 2a). As seen for the Newtonian fluids tested in Fig. 6a, the percentage of fluid removed from the gravure cell was found to increase with the increasing velocity of the top plate, U, until it

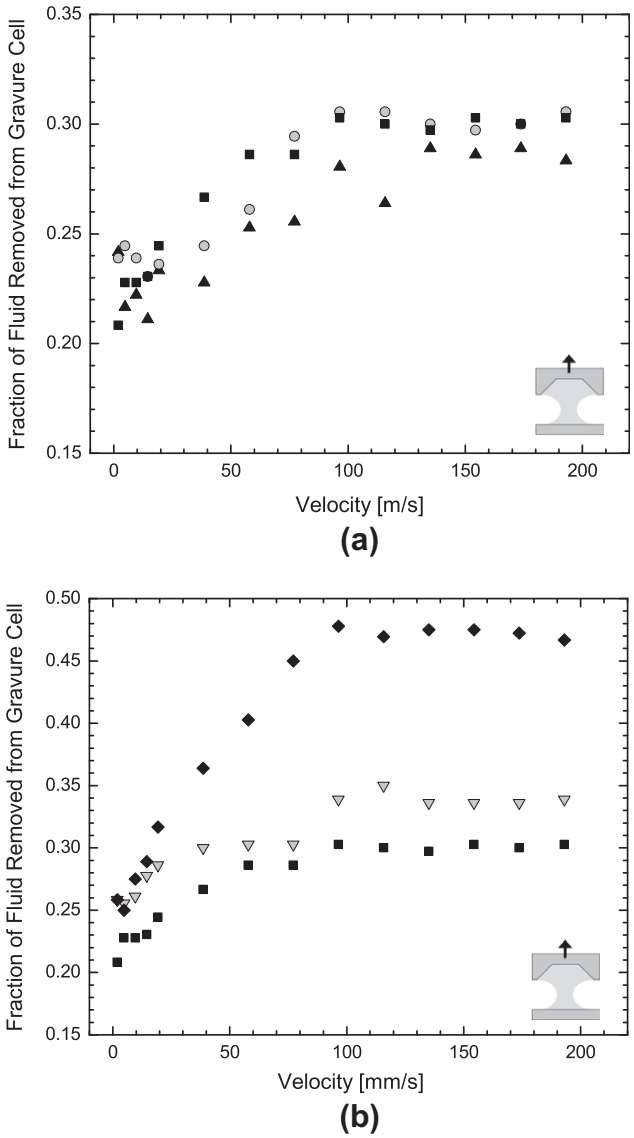

Fig. 10. Fraction of fluid removed from the gravure cell (pickout) as a function of velocity for the configuration where the gravure cell is placed on the top plate and moving. The data include: (■) 20% 20K PEO, (•)15% 20K PEO, (▲) 10% 20K PEO, (▼) 2M PEO and (◆) 8M PEO.

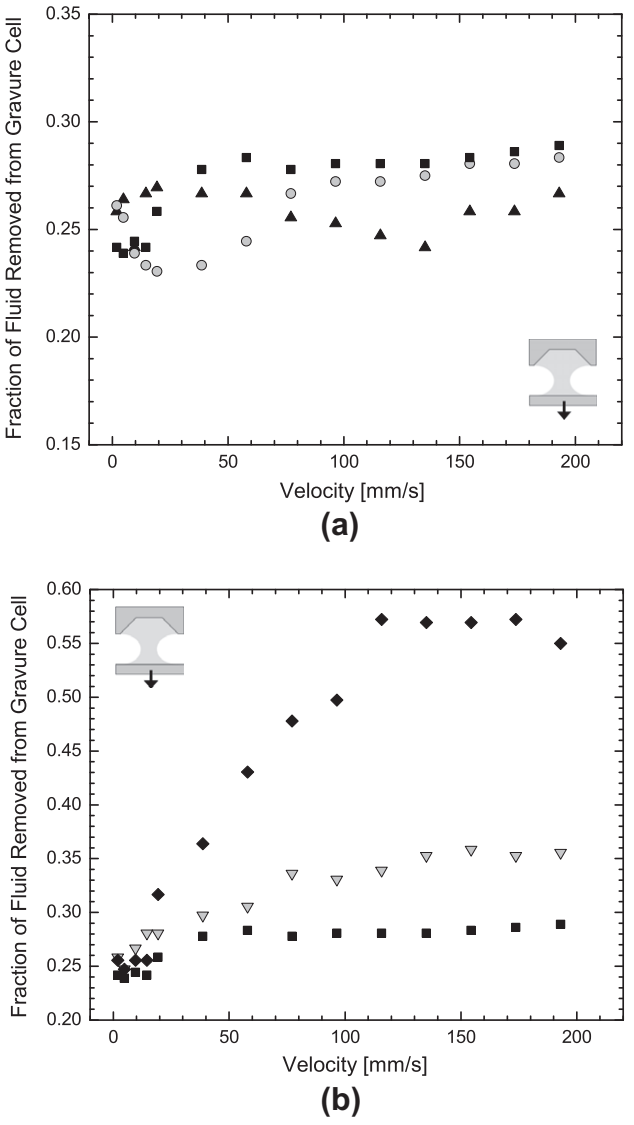

Fig. 11. Fraction of fluid removed from the gravure cell (pickout) as a function of velocity for the configuration where the gravure cell is placed on the top plate and remains stationary. The data include: (■) 20% 20K PEO, (•)15% 20K PEO, (▲) 10% 20K PEO, (▼) 2M PEO and (◆) 8M PEO.

reached a plateau at higher speeds. Over all the stretch velocities that were tested, the 20% 20K PEO was consistently found to remove more fluid from the gravure cell than the lower viscosity 15% or 10% 20K PEO samples. As seen in Table 1, the addition of more low-molecular-weight PEO both decreases the surface tension and increases the shear viscosity. As a result, the capillary number, which is defined as $Ca = \eta_o U/\sigma$ and represents the relative importance of viscous to interfacial stresses, increases with increasing concentration of 20K PEO for any given stretch velocity. If the data is plotted as a function of capillary number, as is done in the inset of Fig. 6a, the data collapse very well onto a single master curve with the exception of the high capillary number regime where the plateau value of the data appears to be dependent on fluid properties.

From high-speed videos, it was observed that the Newtonian fluids do not fully dewet from the sidewalls of the gravure cell at any stretch rate tested. The three-phase contact line remains pinned at the sharp corner entering the gravure cell because sufficient interface curvature is not induced to deform the contact line past the receding contact angle. This can be seen explicitly in the time-series images of the 20 wt% 20K PEO solution presented in Fig. 7. Note the slight asymmetry in the sessile drops on the top and bottom plates. This is a caused by gravity. The Bond number, $Bo = \rho g R^2/\sigma$, describes the relative importance of gravitational forces to interfacial forces. The Bond number at the onset of stretch is approximately $Bo = 0.9$, gravity cannot be neglected and it causes the modest asymmetry in the top and bottom drops seen in Fig. 7. However, it is important to note that at later stages, once the liquid bridge has been formed, the Bond number decreases by several orders of magnitude and the effect of gravity can be neglected in the later stage dynamics. Gravity, for instance, should not induce preferential downward drainage once the liquid bridge has been established.

Note that in this configuration, the fluid that is being deposited on the top plate is primarily from the fluid originating from the gap between the gravure cell and plate, and needed to maintain the initial aspect ratio of $L_i/R = 0.3$. For the 1mm deep cell used here, 40% of the total fluid is between the gravure cell and the plate at this aspect ratio. Preliminary experiments were performed with lower

initial aspect ratios, however, no significant changes were observed in the amount of fluid removed from the gravure cell and so it was decided to use an initial aspect ratio of $L_i/R = 0.3$ because the higher aspect ratio resulted in more repeatable and easier to perform experiments.

As seen in Fig. 6b, with the gravure cell on the bottom and stationary, the viscoelastic fluids tested present a qualitatively different kind of behavior than the Newtonian fluids. The trends of the percentage of fluid removed from the gravure cell for the less elastic 2M PEO solution are qualitatively similar to those of the Newtonian samples. The percentage of fluid removed from the gravure cell is found to increase with increasing stretch velocity before reaching a plateau. The value of the plateau for the 2M PEO sample is lower than the Newtonian fluid, 20% compared to 24%, even though the viscosity of the 2M PEO is twice that of the 20 wt% 20K PEO. This is opposite to the trend with shear viscosity observed for the three Newtonian samples. This suggests that the decrease in fluid removed from the gravure cell is a result of the elasticity and large extensional viscosity of the 2M PEO sample. Increasing the elasticity of the sample changes the response of the fluid even further. Below a stretch velocity of about 25 mm/s, the 8M PEO solution follows the same trends as both the 2M PEO and 20 wt% 20K PEO solutions. However, as the speed of the stretch increases the percentage of fluid removed goes through a maximum and decreases dramatically eventually reaching a plateau of just 5%. If the data in Fig. 6b are replotted against capillary number, all three solutions collapse onto a master curve at small capillary number, but the viscoelastic fluids deviate from the Newtonian response at larger capillary number. For the 2M PEO solution, the deviation occurs above a Ca > 0.05, while for the 8M PEO solution, the deviation occurs above Ca > 0.03.

As the stretch velocity is increased, the strength of the imposed extensional flow increases. We can estimate the extension rate as $\dot{\varepsilon} \simeq U/L$ [34]. Note that because this stretch is at a constant velocity, the extension rate imposed on the liquid bridge decreases linearly with time and stretch length. Hence, in this experiment, the greatest extension rates are imparted on the liquid bridge at the start of the stretch. At $U = 25$ mm/s, where the percentage of the 8M PEO fluid removed from the gravure cell begin to decrease with increasing stretch velocity, the extension rate is such that for the majority of the stretch, the Weissenberg number was greater than one, $Wi > 1$ and elasticity becomes important. This causes initial larger stresses in the fluid filament and, as seen in Figs. 8 and 9, more deformation in the sessile drop on the bottom plate. Still the contact line remains pinned at the edge of the gravure cell and none of the solutions dewet from the gravure cell. As the stretch continues, the diameter of the liquid bridge decays, the elongation rate reduces and the tensile force exerted by the liquid bridge on the sessile drops decays with time. This is true even in filament stretching experiments where the elongation rate remains constant [34]. As a result of the reduction in tensile force, as seen in Figs. 8 and 9, the initially large deformation in the sessile drop diminishes with time and the sessile drop grows as fluid from the liquid bridge drains into the drop. In some cases due to the elasticity of the samples and the finite travel of our linear motor, once the stretch stops there is a fine liquid filament that is formed between the plate and the cell which is similar to those seen in CaBER experiments. This liquid bridge is typically only several tens of microns and because the Bond number is small at this point it drains equally into the top and bottom sessile drop through capillary drainage.

3.2. Printing with gravure cell on the top and moving

In order to investigate the role of gravity and inertia in the pickout process, the gravure cell was mounted to the motor and moved upward while keeping the flat plate stationary at the bottom. In this configuration, which can be seen schematically in Fig. 2b, the direction of both the gravitational and the inertial forces on the fluid have been reversed. The initial conditions aspect ratio and the range of stretch speeds were kept fixed. The percentage of fluid removed from the gravure cell in this configuration is shown in Fig. 10 for both the Newtonian and viscoelastic fluids. The trend for a Newtonian fluid is similar to the previous configuration. As seen Fig. 10a, the percentage of fluid removed from the gravure cell was found to increase with the increasing velocity of the top plate until it reached a plateau at higher speeds. If replotted against capillary number, as before, the data collapse well. The higher viscosity fluid was again found to result in an increase in fluid removed from the gravure cell, although the difference between fluids is not as significant as it was in the previous configuration. For the Newtonian fluids, the plateau value of the pickout was found to increase by about 5% to about 30%. This is likely due to the initial slight asymmetry in the shape of the liquid bridge cause by gravity. Unfortunately, in this configuration, high-speed videos were not possible because the gravure cell moved out of the frame before the evolution of the contact line could be observed.

Unlike the Newtonian case, the percentage of viscoelastic fluid removed from the gravure cell in this configuration was found to demonstrate a very different trend. Where in the first configuration, with the gravure cell on the bottom, viscoelasticity was found to reduce the percentage of fluid removed from the gravure cell, in this configuration, with the gravure cell on the top and moving, viscoelasticity was found to greatly enhance the percentage of fluid removed from the gravure cell. This can be seen explicitly in Fig. 10b. For both viscoelastic fluids, the percentage of fluid removed from the gravure cell increases with increasing stretch velocity before reaching a plateau. For the 2M PEO solution, that plateau is at 34%, while for the 8M PEO solution, the plateau is at

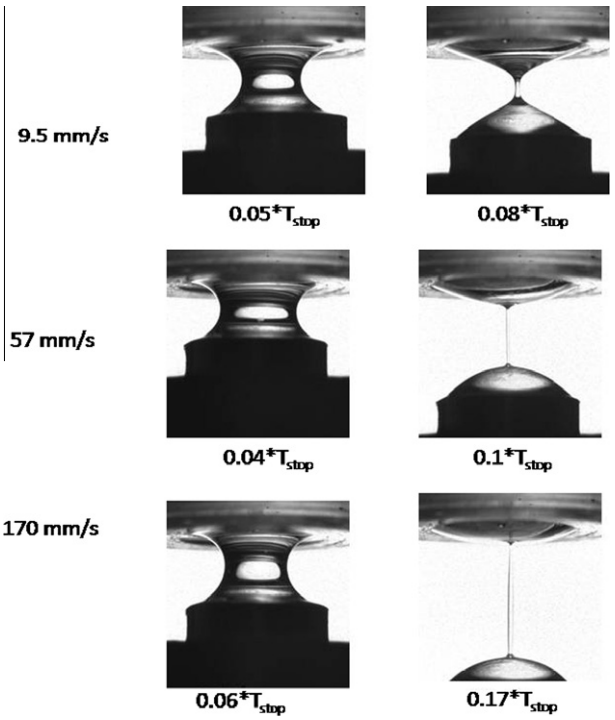

Fig. 12. Time series of images of 20% 20K PEO dewetting when the gravure cell is held stationary as the top plate. Time is non-dimensionalized with the time that the bottom plate reaches the end of its travel and stops, T_{stop}. For the three stretch velocities shown here from top to bottom, $T_{stop} = 3.2$ s, 0.53 s and 0.18 s.

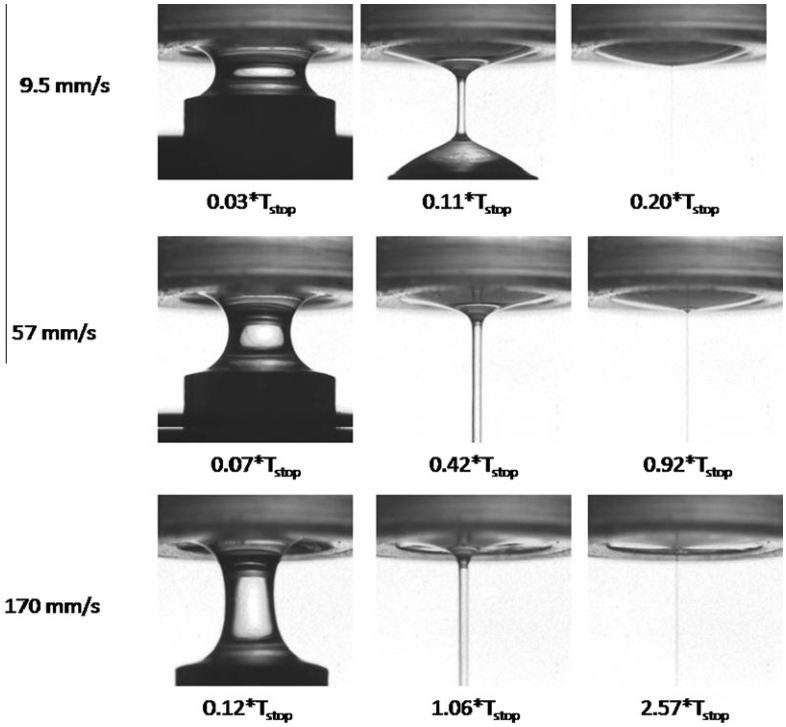

Fig. 13. Time series of images of 2M PEO dewetting when the gravure cell is held stationary as the top plate. Time is non-dimensionalized with the time that the bottom plate reaches the end of its travel and stops, T_{stop}. For the three stretch velocities shown here from top to bottom, T_{stop} = 3.2 s, 0.53 s and 0.18 s.

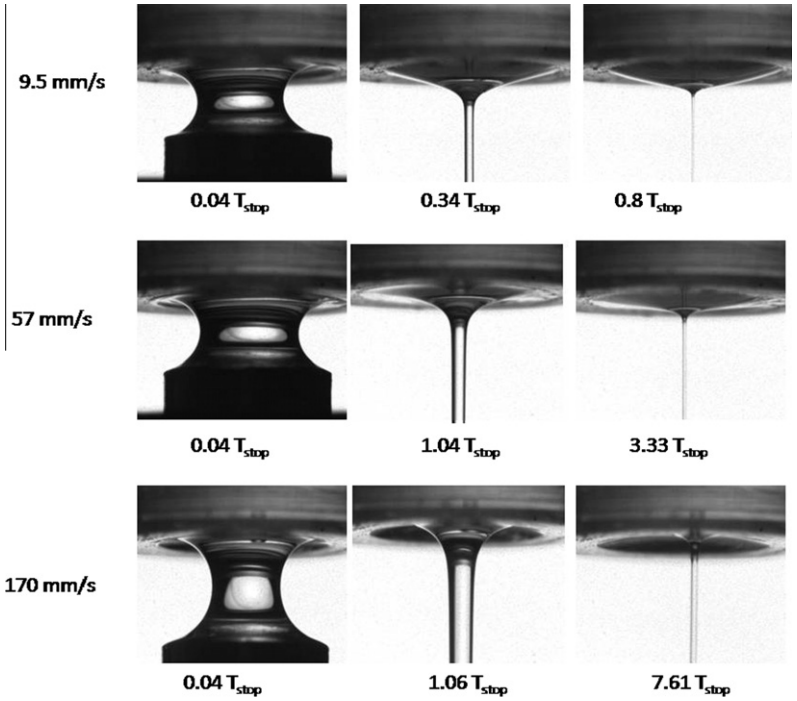

Fig. 14. Time series of images of 8M PEO dewetting when the gravure cell is held stationary as the top plate. Time is non-dimensionalized with the time that the bottom plate reaches the end of its travel and stops, T_{stop}. For the three stretch velocities shown here from top to bottom, T_{stop} = 3.2 s, 0.53 s and 0.18 s.

nearly 50%. Compare that to the 30% removal of fluid achieved by the most viscous Newtonian fluid or perhaps more interestingly the 5% removal of fluid for the 8M PEO solution in the previous configuration. Again the data tend to collapse if replotted against capillary number. The deviation of the 2M PEO and the 8M PEO solutions occur roughly at the same stretch velocities and Weissenberg numbers demonstrating conclusively that the difference between the high and low molecular weight PEO solutions is fluid

elasticity. What remains unclear is what caused the qualitative difference in the pickout between these two configurations, gravity or inertia.

3.3. Printing with gravure cell on top and stationary

In order to isolate the effect of inertia in the pickout process, the gravure cell was mounted to top plate and the motor was rotated 180° and mounted upside down to the bottom plate. As a result, in this configuration, the motor could impose a constant downward velocity while allowing the gravure cell to be held stationary. In this configuration, which can be seen schematically in Fig. 2c, the direction of the inertial forces has been reversed from the previous direction while keeping the direction of the gravitational force fixed. The percentage of fluid removed from the gravure cell in this configuration is shown in Fig. 11. The trend for a Newtonian fluid changing the inertial direction has very little effect. Perhaps the only change observed in Fig. 11a is a slight reduction in the plateau value of the percentage of fluid removed from the gravure cell, but that variation is within the uncertainty of these experiments. The high-speed images shown in Fig. 12 demonstrate that flow is not strong enough for any of the Newtonian fluids to result in a dewetting of the three-phase contact line from the corner of the gravure cell.

As seen in Figs. 13 and 14, the same cannot be said for the viscoelastic test fluids. At low stretch velocities, the three phase contact line remains pinned at the corner of the gravure cell. However, for both the 2M PEO and the 8M PEO fluids, as the stretch velocity is increased the contact line becomes unpinned from the corner and advanced into the gravure cell. The depth of this advance was found to be dependent on both the stretch velocity and the fluid with increased stretch velocity and fluid elasticity causing more dewetting. In some cases, as the liquid bridge drained, the gravure cell was partially or fully refilled. For both the 2M PEO and the 8M PEO fluids, this configuration results in the largest percentage of fluid, 36% and 57% respectively, being transferred from the gravure cell. That represents a roughly 10% improvement over the previous configuration that is due to the effect of inertia. The role of inertia is often quantified by the Reynolds number, $Re = \rho UR/\eta_0$, which compares the relative strength of inertial forces to viscous forces. At the low stretch velocities presented in Fig. 11, the Reynolds number is typically $Re \ll 1$ and inertial effects can be neglected and the data for this and the previous configuration overlap. However, at the largest stretch velocities, the Reynolds number in these experiments can grow to between $2 < Re < 45$ depending on the viscosity of the fluid used. At these Reynolds numbers, inertia cannot be neglected and the data for this and the previous configuration diverge. Similar trends with increasing Reynolds number were observed by Dodds et al. [12] who used numerical simulations to study the effect of inertia on the pickout process for Newtonian fluids. They showed that increasing Reynolds number resulted in an increase in the fluid removed from a gravure cell and changed the break up dynamics of the liquid bridge away from a symmetric breakup that occurred simultaneously at both the top and bottom sessile drop to one which was anti-symmetric and occurred at the sessile drop attached to the stationary wall. A similar transition in breakup dynamics can be seen in Fig. 12, for the 20 wt% 20K PEO solution as the stretch velocity is increased. Unfortunately, the fluid filament was too long-lived for both the 2M PEO and the 8M PEO solutions to determine if a similar transition occurs for viscoelastic fluids because the moving plane and stationary plate could not be maintained in view simultaneously with adequate resolution to visualize the breakup dynamics.

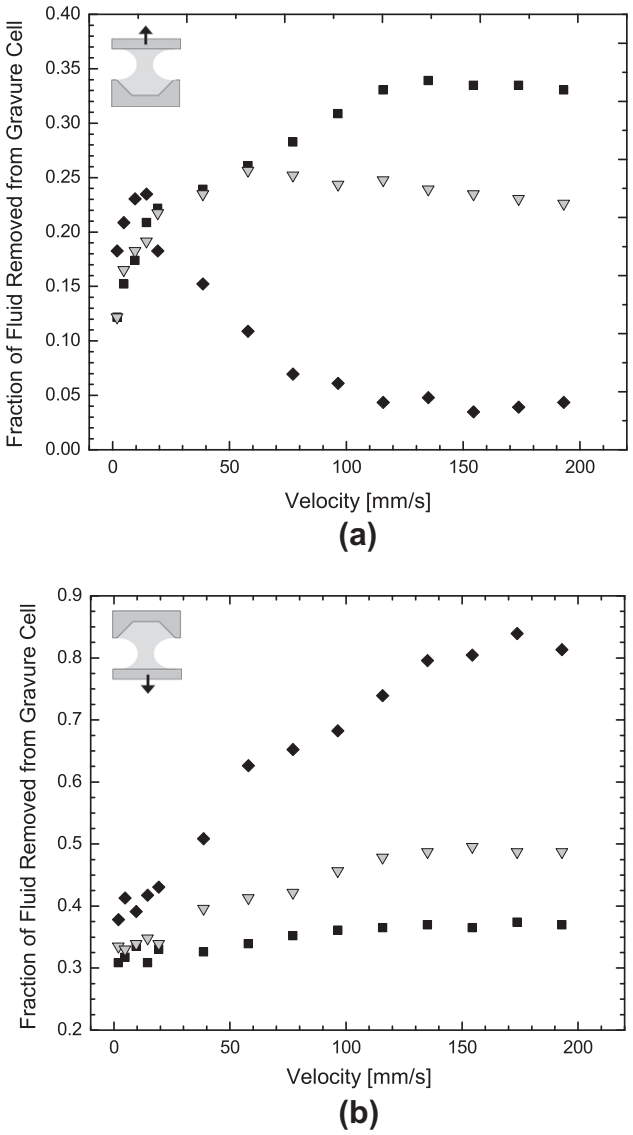

Fig. 15. Fraction of fluid removed from the gravure cell (pickout) as a function of velocity for the shallow ($h/R = 0.1$) gravure cell. The data include: (■) 20% 20K PEO, (▼) 2M PEO and (◆) 8M PEO for configuration where the gravure cell is placed on (a) the bottom plate and with the top plate moving and (b) the top plate with the bottom plate moving.

3.4. Effect of gravure cell geometry on printing

The specific geometry of the gravure cell can have a significant impact on the pickout process. The two major geometric modifications that can be studied are the effect of varying the angle of the sidewalls of the gravure cell, α, and the aspect ratio of the gravure cell, h/R. By reducing the angle of the sidewalls of the gravure cell, dewetting of the gravure cell can be enhanced by making it easier for the sessile drop to reach its receding contact angle on the sidewall and unpin from the corner of the gravure cell. As seen in the previous section, a sidewall angle of $\alpha = 15°$ was sufficient to facilitate dewetting of the 8M PEO solution. However, even though the aspect ratio of the gravure cell was relatively small, $h/R = 0.2$, a maximum of only 60% of the fluid was transferred from the gravure cell to the flat plate. To understand the impact of aspect ratio, a series of experiments were performed using a gravure cell with an aspect ratio of $h/R = 0.1$. The results of these experiments are presented in Fig. 15 for the configurations where the gravure cell is placed either on the bottom (Fig. 15a) or the top plate

(Fig. 15b) and held stationary while the flat plate moves away at a constant velocity. The percentage of fluid removed from the lower aspect ratio gravure cell significantly larger than from the higher aspect ratio gravure cell for both configurations and each of the test fluids used. The most dramatic improvement is observed for the 8M PEO solution in Fig. 15b for which nearly 90% of the fluid is removed from the lower aspect ratio gravure cell.

4. Conclusions

In this study, we have shown that there are a number of factors that can greatly affect the gravure printing process. These factors, which include gravure cell geometry, stretch velocity, gravity, inertia, capillarity and viscoelasticity, can each have a dramatic affect on the printing process by altering the evolution and breakup of the liquid bridge that is formed and then stretched between an idealized gravure cell and a flat plate. As a result, these factors can greatly influence the total amount of fluid transferred from the gravure cell. In this study, we focused on the effect that viscoelasticity of the test fluid can have on gravure printing. Two different fully characterized viscoelastic fluids were developed with varying degrees of elasticity along with a series of Newtonian fluids with different viscosities. For the Newtonian fluids, the percentage of fluid transferred from the gravure cell initially increased with increasing stretch velocity before reaching a plateau at higher stretch velocities. The value of the plateau was found to increase with increasing fluid viscosity. However, when the data was replotted as a function of capillary number instead of stretch velocity, the data from all three Newtonian fluids was found to collapse onto a single master curve at low capillary numbers before deviating at high capillary numbers where the plateau was reached. A number of different configurations of the gravure cell and flat plate were studied including the gravure cell on top and bottom, stationary and moving. For the Newtonian fluids, the configuration of the gravure cell did not have a qualitative impact on the amount of fluid transferred from the gravure cell. In all cases, the three-phase contact line remained pinned at the corner of the gravure cell and the fluid never fully dewetted. The maximum fluid transfer was achieved with the gravure cell on the top and stationary and the plate moving downward away from the cell. In this configuration, at the higher stretch speeds tested, fluid inertia was found to affect the shape of the liquid bridge, breaking its symmetry and causing it to pinch off from the sessile drop attached to the gravure cell.

The viscoelastic fluids showed a very different, more complicated response. At low stretch velocities, the behavior of the viscoelastic fluids mirrored the response of the Newtonian fluids. However, as the stretch velocity and subsequently the Weissenberg number were increased, elastic effects were found to dominate. The observed effect of viscoelasticity was found to be strongly dependent on the experimental configuration. With the gravure cell on the bottom and the top plate moving upward increasing elasticity was found to decrease the amount of fluid transferred from the gravure cell. In fact, for the most elastic fluid, the amount of fluid transferred initially increased with increasing stretch velocity before going through a maximum and reaching a plateau at larger stretch velocities where only 5% of the fluid was transferred to the flat plate. This maximum in the fluid transfer was found to occur at a stretch velocity which resulted in a Weissenberg number of $Wi > 1$ for more than half the stretch. At these Weissenberg numbers, elastic effects become important. In this configuration, gravity and the resulting sagging of the liquid bridge were also found to be important. When, however, the experiment and gravity were flipped over and the gravure cell was placed on the top plate with the flat bottom plate moving downward, a very different trend was observed. The data no longer went through a maximum. Instead, the amount of fluid transferred from the gravure cell was found to increase with increasing stretch velocity before reaching a plateau and, more interestingly, the value of the plateau was found to increase significantly with increasing fluid elasticity. In this configuration, for the most elastic fluid, nearly 60% of the fluid was transferred from the gravure cell. Compare that to less than 30% transfer from the most viscous Newtonian fluid. High-speed time lapse images demonstrated that for the viscoelastic fluids in this configuration, the increased fluid transfer is directly related to the unpinning of the three phase contact line from the corner of the gravure cell and the partial dewetting that occurred during the stretch. Furthermore, it was shown that by reducing the aspect ratio of the gravure cell by a factor of two, that for the most elastic liquid that nearly 90% of the fluid could be transferred from the gravure cell. These observations clearly show that viscoelasticity can have an enormous effect on gravure printing.

Acknowledgement

This work was supported by NSF Center for Hierarchical Manufacturing at UMASS under Grant numbers CMMI-0531171 and CMMI-1025020.

References

[1] S.H. Ahn, L.J. Guo, Large-area roll-to-roll and roll-to-plate nanoimprint lithography: a step toward high-throughput application of continuous nanoimprinting, ACS Nano 3 (2009) 2304–2310.
[2] D. Lucas, J.-S. Kim, C. Chin, L.J. Guo, Nanoimprint lithography based approach for the fabrication of large-area, uniformly oriented plamonic arrays, Adv. Mater. 20 (2008) 1129–1134.
[3] N. Hoda, S. Kumar, Boundary integral simulations of liquid emptying from a model gravure cell, Phys. Fluids 20 (2008) 092106.
[4] T.-M. Lee, J.-H. Noh, I. Kim, D.-S. Kim, S. Chun, Reliability of gravure offset printing under various printing conditions, J. Appl. Phys. 108 (2010) 1–6.
[5] D.H. Ahmed, H.W. Kang, H.J. Sung, Non-Newtonian effect on ink transfer for gravure offset printing, in: IEEE International Symposium on Assembly and Manufacturing, Suwon, Korea, 2009.
[6] S. Dodds, M. da Silveira Carvalho, S. Kumar, Stretching and slipping of liquid bridges near plates and cavities, Phys. Fluids 20 (2009) 092103.
[7] N.H.a.S. Kumar, Boundary integral simulations of liquid emptying from a model gravure cell, Phys. Fluids 20 (2008) 1–12.
[8] M. Pudas, S. Leppävuori, J. Hagberg, The absorption ink transfer mechanism of gravure offset printing for electronic circuitry, IEEE Trans. Electron. Pack. Manuf. (2002).
[9] C.A. Powell, M.D. Savage, J.T. Guthrie, Computational simulation of the printing of Newtonian liquid from a trapezoidal cavity, Int. J. Numer. Methods Heat Fluid Flow 12 (2002) 338–355.
[10] S. Ahn, S. Lee, Y. Na, Elasticity effect on the ink transfer process in gravure printing, Comput. Sci. Appl. (2008).
[11] S. Dodds, M.d.S. Carvalho, S. Kumar, Stretching and slipping of liquid bridges near plates and cavities, Phys. Fluids 21 (2009).
[12] S. Dodds, M. da Silveira Carvalho, S. Kumar, Stretching liquid bridges with moving contact lines: the role of inertia, Phys. Fluids 23 (2011) 092101.
[13] F. Ghadiri, D.H. Ahmed, H.J. Sung, E. Shirani, Non-Newtonian ink transfer in gravure-offset printing, Int. J. Heat Fluid Flow 32 (2011) 308–317.
[14] N. Hoda, S. Kumar, Boundary integral simulations of liquid emptying from a model gravure cell, Phys. Fluids 20 (2008) 1–12.
[15] W.-X. Huang, S.-H. Lee, H.J. Sung, T.-M. Lee, D.-S. Kim, Simulation of liquid transfer between separating walls for modeling micro-gravure-offset printing, Int. J. Heat Fluid Flow 29 (2008) 1436–1446.
[16] H.W. Kang, H.J. Sung, T.-M. Lee, D.-S. Kim, C.-J. Kim, Liquid transfer between two separating plates for micro-gravure-offset printing, J. Micromech. Microeng. 19 (2009) 1–9.
[17] K. Kim, T. Nam, Y. Na, Analysis of ink transfer process for R2R printing applications with non-newtonian ink property, in: International Conference on Control Automation and Systems IEEE, Gyeonggi-do, Korea, 2010.
[18] J.M. Noyola, M. Pekurovsky, R. Selor, C. Evertz, V. Beck, A continuing study of the effect of rheological properties in gravure coating, in: 10th International Coating Science and Technology Symposium, Scottsdale, Arizona, 2000.
[19] L. Schwartz, P. Moussalli, P. Campbell, R. Eley, Numerical modelling of liquid withdrawal from gravure cavities in coating operations, Trans. IChemE, Part C 76 (1998) 22–28.
[20] L.W. Schwartz, Numerical modeling of liquid withdrawal from gravure cavities in coating operations; the effect of cell pattern, J. Eng. Math. 42 (2002) 243–253.

[21] X. Yin, S. Kumar, Lubrication flow between a cavity and a flexible wall, Phys. Fluids 17 (2005) 1–13.
[22] X. Yin, S. Kumar, Flow visualization of the liquid-emptying process in scaled-up gravure grooves and cells, Chem. Eng. Sci. 61 (2006) 1146–1156.
[23] L.E. Rodd, T.P. Scott, J.J. Cooper-White, G.H. McKinley, Capillary break-up rheometry of low-viscosity elastic fluids, Appl. Rheol. 15 (2005) 12–27.
[24] S.L. Anna, G.H. McKinley, Elasto-capillary thinning and breakup of model elastic liquids, J. Rheol. 45 (2001) 115–138.
[25] G.H. McKinley, A. Tripathi, How to extract the Newtonian viscosity from capillary breakup measurements in a filament rheometer, J. Rheol. 44 (2000) 653–670.
[26] M. Stelter, G. Brenn, A.L. Yarin, R.P. Singh, F. Durst, Validation and application of a novel elongational device for polymer solutions, J. Rheol. 44 (2000) 595–616.
[27] V.M. Entov, E.J. Hinch, Effect of a spectrum of relaxation times on the capillary thinning of a filament of elastic liquid, J. Non-Newtonian Fluid Mech. 72 (1997) 31–53.
[28] A.V. Bazilevsky, V.M. Entov, A.N. Rozhkov, Liquid filament microrheometer and some of its applications, in: D.R. Oliver (Ed.), Proceedings of Third European Rheology Conference, Edinburgh, 1990.
[29] J.P. Plog, W.M. Kulicke, C. Clasen, Influence of the molar mass distribution on the elongational behaviour of polymer solutions in capillary breakup, Appl. Rheol. 15 (2005) 28–37.
[30] C. Clasen, J.P. Plog, W.M. Kulicke, M. Owens, C. Macosko, L.E. Scriven, M. Verani, G.H. McKinley, How dilute are dilute solutions in extensional flows?, J Rheol. 50 (2006) 849–881.
[31] B. Yesilata, C. Clasen, G.H. McKinley, Nonlinear shear and extensional flow dynamics of wormlike surfactant solutions, J. Non-Newtonian Fluid Mech. 133 (2006) 73–90.
[32] N. Kojic, J. Bico, C. Clasen, G.H. McKinley, Ex vivo rheology of spider silk, J. Exp. Biol. 209 (2006) 4355–4362.
[33] D.T. Papageorgiou, On the breakup of viscous liquid threads, Phys. Fluids 7 (1995) 1529–1544.
[34] G.H. McKinley, A decade of filament stretching rheometry, in: Proceedings of XIIIth International Congress of Rheology, 2000.